Tunable Formation of Ordered Wrinkles in Metal Films with Controlled Thickness Gradients Deposited on Soft Elastic Substrates

Senjiang Yu,*,[†] Yong Ni,*,[‡] Linghui He,[‡] and Quan-Lin Ye[§]

[†]Department of Physics, China Jiliang University, Hangzhou 310018, P. R. China

[‡]Department of Modern Mechanics, CAS Key Laboratory of Mechanical Behavior and Design of Materials and Collaborative Innovation Center of Suzhou Nano Science and Technology, University of Science and Technology of China, Hefei, Anhui 230026, P. R. China

[§]Hangzhou Key Laboratory of Quantum Matter, Department of Physics, Hangzhou Normal University, Hangzhou 310036, P. R. China

S *Supporting Information*

ABSTRACT: Controlled wrinkled surface is useful for a wide range of applications, including flexible electronics, smart adhesion, wettability, stamping, sensoring, coating, and measuring. In this work, thickness-gradient-guided spontaneous formation of ordered wrinkling patterns in metal films deposited on soft elastic substrates is revealed by atomic force microscopy, theoretic analysis, and simulation. It is observed that in the thicker film region, broad cracks form, and the film surface remains flat. In the thinner film region, the cracks attenuate along the direction of the thickness decrease, and various wrinkle patterns including branched stripes, herringbones, and labyrinths can coexist. The interplay between the residual compression and the thickness gradient leading to the formation of such wrinkling patterns is discussed based on a nonlinear wrinkling model. The simulated wrinkling patterns as well as the variation trends of the wrinkle wavelength and amplitude along the gradient direction are in good agreement with the experimental observations. The report in this work could promote better understanding and fabrication of such ordered wrinkling patterns by tunable thickness gradient.

KEYWORDS: *buckling instability, pattern formation, wrinkle, thickness gradient, thin films*
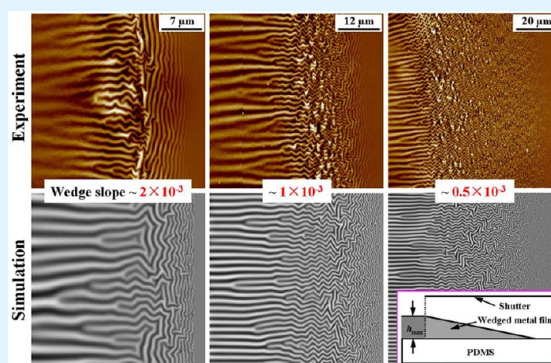
I. INTRODUCTION

Wrinkled surfaces have been widely observed both in nature and emergent technology.[1−3] It usually develops from a wrinkling instability of a hard layer beyond a critical compression on soft substrates.[3−5] The surface topography with various patterns can be dynamically regulated in a large area. Such shape tunability of the surface exhibits many potential applications[6] including flexible electronics,[7] microfluidic channel,[8] smart adhesion,[9,10] wettability,[11] measurement of thin-film properties,[12] elastomeric optics,[13] smart coating for marine antifouling,[14] photonics,[15] mechanosensitivity,[16] and self-assembly ordered microstructures.[17] To elaborate the applications extensive studies have explored possible ways of manipulating the compression in the film and thus to generate the controlled wrinkling patterns. The compression can be regulated by thermal expansion mismatch,[18−20] swelling of solvent diffusion into the film,[21−25] phototriggered structural transformation,[26,27] capillarity,[28] and bubble inflation in the film.[29] It is known that uniaxial compression in the film induces stripe wrinkles, while isotropic compression usually induces randomly oriented labyrinth wrinkling patterns or ordered herringbone patterns.[30−34] Recently it was reported that the

transition from disordered to ordered wrinkling patterns with some directional preference occurs from a symmetry breaking triggered by the compression anisotropy.[35−37] The ordered herringbone patterns with tunable long wavelength and jog angle different than 90° can be created via progressively released biaxial strain. In addition, ordering wrinkling patterns can also be tuned by other ways of symmetry breaking, such as the confinement of a prepatterned substrate,[38] the selective interfacial adhesion between the film and the substrate,[39] the spatially sequential wrinkling,[40] the constrained edge effect,[41,42] etc.

In this paper, we show a different symmetry breaking of the wrinkling patterns caused by the tunable thickness gradient in metal films deposited on soft elastic (polydimethylsiloxane, PDMS) substrates. The film is prepared via magnetron sputtering technique at room temperature. The thickness gradient is controlled by placing a shutter between the substrate and the target during film deposition. The tunability of the

thickness gradient is realized by changing the distance between the substrate and the shutter. Although the wrinkling formation in a uniaxially compressed thin film with a preexisting gradient thickness bounded on soft substrates was experimentally and theoretically reported,[43−46] the interplay between biaxial compression and tunable thickness gradient on the nonlinear wrinkle formation remains unclear. In the presence of the thickness gradient, the wrinkling pattern that seems under uniaxial compression can still form even if the precompression in the film is equally biaxial. Furthermore, the equilibrium wrinkling wavelength and amplitude are no longer spatially uniform. The wrinkling patterns obtained here are hierarchically ordered different from the uniform wrinkling patterns reported in most previous studies.

Our experiment shows that after the thickness gradient film is cooled, the residual compressive strain generated due to thermal expansion mismatch is isotropic. However, the resultant compressive stress of the film becomes positionally dependent anisotropic in the presence of tunable thickness gradient. Spontaneous formation of ordered wrinkles with coexisting branched straight stripes, herringbones, and labyrinths along the direction of the thickness gradient has been observed and characterized by atomic force microscopy (AFM). By performing a numerical simulation based on the model of Föppl-von Kármán (FvK) plates[47] with residual strain and different thickness gradients on elastic foundations,[23,48] the formation mechanism of the thickness-gradient dependent wrinkle patterns is elucidated by theoretic analysis. The simulated nonlinear wrinkling morphologies are in good agreement with the AFM observations. The results also provide the ability to generate such hierarchically ordered wrinkles via regulation of the thickness gradient.

II. EXPERIMENTAL SECTION

Materials. The gel and cross-linker of PDMS (Dow Corning's Sylgard 184) were mixed with 10:1 volume ratio. Then the PDMS was spin-coated onto clean glass slides with the areas of ∼10 × 10 mm². The substrates were cured for 4 h at 80 °C and then naturally cooled in air. The resulting PDMS substrates had the thickness of ∼20 μm. The sputtering target was a piece of nickel or iron disk (purity 99.9%) with a diameter of 60 mm and a thickness of 3 mm.

Film Fabrication. The film samples were prepared by direct current (DC) magnetron sputtering at room temperature. The target-substrate distance was ∼80 mm. The base pressure was below 2×10^{-4} Pa and the working argon gas (purity 99.99%) pressure was 0.5 Pa. The DC sputtering power was fixed to be 56 W, corresponding to the deposition rate of ∼15 nm/min. The deposition time ranged from 10 s to 20 min, which was controlled precisely by a computer. After deposition, the film thickness was measured by a profilometer (Dektak-XT). The film thickness can be tuned easily by changing the deposition time. To fabricate thickness-gradient metal films, a stainless steal shutter with 10 mm length, 3 mm width, and 0.2 mm thickness was placed between the PDMS substrate and the target during deposition. The distance between the shutter and the substrate was varied from zero to several millimeters. The slope of the wedged film was determined by the maximum film thickness and the wedge width.

Characterization. The surface morphologies of the samples were observed and taken by an optical microscope (Leica DMLM) equipped with a charge-coupled device camera. The wrinkle morphologies and profile structures were scanned by an atomic force microscope (AFM, XE-100E, psia) operated in noncontact or tapping mode. Collected data consisted of height information on square 256 × 256 arrays of pixels from area scans with lengths from 5 to 90 μm.

III. RESULTS AND DISCUSSION

The thickness-gradient metal film (here is nickel) deposited on the PDMS substrate was prepared by placing a shutter between the substrate and the target during deposition, as shown in Figure 1a. Because of the collision by the gas molecules and
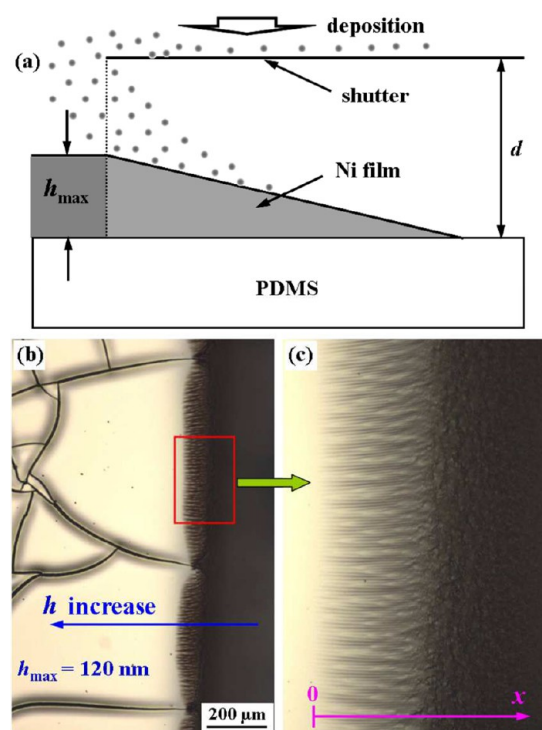
Figure 1. (a) Schematic view of the cross section of a thickness-gradient film prepared by placing a shutter between the substrate and the target during deposition. (b) Typical surface morphology of the thickness-gradient film on the PDMS substrate taken by the optical microscopy. The blue arrow represents the increase in the film thickness. The maximum film thickness is 120 nm in this case, and the distance from the shutter to PDMS substrate is ∼2 mm. (c) Enlarged view of the red box in Figure 1b. The x-axis is starting from the appearance of the winkling patterns. Note that the x-axis denotes the decrease in the film thickness.

other particles, some of the metal atoms can deposit onto the PDMS surface behind the shutter. As a result, a thickness-gradient film naturally forms near the shutter edge. The thickness-gradient reflected as the slope of the film is closely dependent on the distance d: larger value of d corresponds to smaller slope. During the deposition, the temperature of the PDMS substrate would increase obviously owing to the heat radiation and particle bombardment. As a result, the PDMS substrate thermally expands and places the metal film under a tensile stress. This tensile stress increases approximately linearly with the deposition time. When the tensile stress is beyond a critical value, cracks start to form in the brittle film, as shown in Figure 1b. The number and width of the cracks increase gradually during deposition to release more stress energy. After the deposition, when the sample cools to the ambient temperature, the PDMS substrate thermally contracts and places the metal film under a compressive stress. If the film thickness is much larger, a large number of broad cracks form during the deposition. These cracks separate the film into isolated islands. If the island is smaller than a critical value, the compression can be released by in-plane relaxation from the
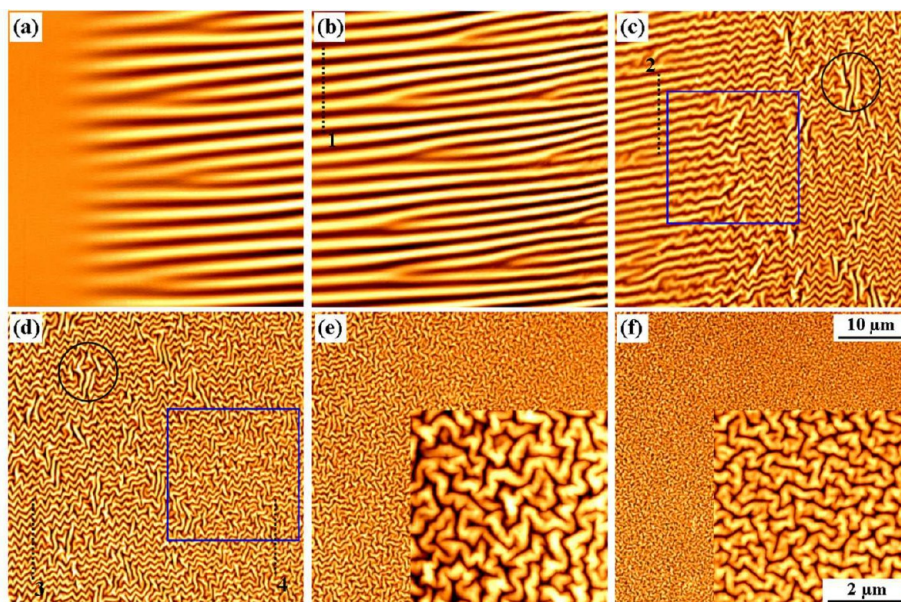
Figure 2. Sequential profiles of the wrinkling patterns with increasing the distance x taken by AFM. (a−f) The images start from x = 0, 45, 90, 135, 180, and 225 μm, respectively. The circles in Figures 2c,d denote the vertically aligned stripe wrinkle segments. All AFM images have the sizes of 45 × 45 μm^2. (insets) The enlarged views of the labyrinth wrinkles with the size of 5 × 5 μm^2.

crack edge, and the wrinkle is not energetically favorable. However, if the film thickness is very small, no crack forms in the film, and therefore the compressive stress is relieved by formation of wrinkling patterns (Figure 1c). Similar wrinkling patterns can be found in a variety of thickness-gradient metal films, including nickel, iron, chromium, aluminum, etc.

To investigate more details of the wrinkled surface of the thickness-gradient film, sequential AFM images were taken as the distance x indicated in Figure 1c increases. The typical results are shown in Figure 2. Clearly, the wrinkling patterns show a hierarchical profile with coexisting branched straight stripes, followed by herringbones and labyrinths along the direction of the thickness decrease. In Figure 2a near the position of x = 0, there is no wrinkling pattern because most compression has been released by the free edge due to the cracks. When the distance x increases, stripe wrinkles parallel to the direction of the thickness gradient arise. The wrinkle wavelength decreases gradually via wrinkle branching as shown in Figure 2b. After the distance is beyond a certain value (∼80 μm in Figure 2c), the straight stripes start to destabilize and evolve into herringbone patterns gradually. The transition from stripes to herringbones is enlarged and shown in Supporting Information, Figure S1a. In addition, vertically aligned stripe wrinkle segments, which favor the release of the compression in the x-axis, can be observed in the areas marked by the circles in Figures 2c,d. In Figure 2d, the wrinkles become randomly oriented, resulting in the formation of labyrinthlike patterns. The transition from herringbones to labyrinths is enlarged and shown in Supporting Information, Figure S1b. Supporting Information, Figure S1c plots four corresponding AFM profiles of the wrinkles at different positions indicated in Figure 2. It is shown that the stripes and herringbones are both well-periodic, whereas the labyrinth wrinkles are randomly oriented. The wrinkle wavelength decreases obviously from profiles 1 to 4, but the amplitude changes slightly. It can be seen from Figure 2e,f that the labyrinths attenuate gradually with increasing the distance x, resulting in the indiscernibility of these patterns. The insets of Figure 2e,f show two enlarged views of the

labyrinths. The evolution of the labyrinths with decreasing the film thickness is shown in Supporting Information, Figure S2. Clearly, the wrinkle dimensions decay successively, but the labyrinth morphologies are self-similar. When x > 350 μm, the discontinuous film forms, and thus the labyrinth wrinkles disappear. When x > 400 μm, the metal atoms are hardly deposited on this region, and pure PDMS surface emerges.

To understand the formation of such complex wrinkling patterns, it is necessary to take into account nonlinear film deformation. We model the compressed film with thickness gradient along x-axis on soft elastic substrates as a thickness-gradient FvK plate with residual compression mounted on elastic substrates.[48] The profile of the deformed film surface is characterized by the middle-plane displacement of the plate $\mathbf{u}$ = (u_α, ζ). The equilibrium wrinkling morphology is the result of the mechanical equilibriums for the film in the in-plane direction

$$N_{\alpha\beta,\beta} = T_\alpha^s \tag{1}$$

and in the normal direction

$$\nabla^2(D(x)\nabla^2\zeta) - (N_{\alpha\beta}\zeta_{,\alpha})_{,\beta} + T_3^s = 0 \tag{2}$$

where the membrane force $N_{\alpha\beta}$ is a function of the membrane strain $e_{\alpha\beta}$, which can be expressed by the middle-plane displacement $\mathbf{u}$.

$$N_{\alpha\beta} = \bar{E}_f(x)[(1 - \nu_f)e_{\alpha\beta} + \nu_f e_{\gamma\gamma}\delta_{\alpha\beta}] \tag{3}$$

$$e_{\alpha\beta} = \frac{1}{2}(u_{\alpha,\beta} + u_{\beta,\alpha}) + \frac{1}{2}\zeta_{,\alpha}\zeta_{,\beta} - \varepsilon_{\alpha\beta}^0(x) \tag{4}$$
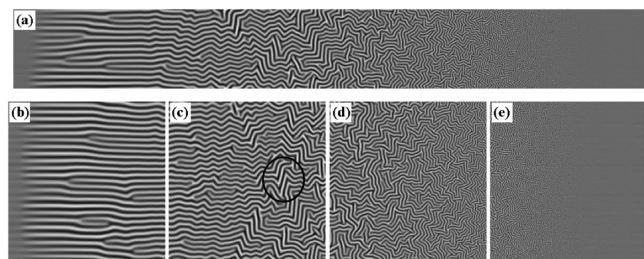
T_i^s is the interfacial traction component on the substrate surface and can be expressed as a function of the displacement component u_i^s on the substrate surface by using the Green function method and also as a function of the middle-plane displacement $\mathbf{u}$ = (u_α, ζ) according to the geometry condition $\mathbf{u}^s$ = $\mathbf{u}$ across the interface between the film and the substrate.[23,30] $\bar{E}_f(x)$ = $2h(x)\mu_f/(1-\nu_f)$ is the effective stiffness of the

membrane force, $D(x) = \mu_f h(x)^3/[6(1-\nu_f)]$ is the position-dependent bending rigidity of the film with $h(x)$ the local thickness, μ_f and ν_f the shear modulus and Poison ratio of the film, respectively. $\varepsilon_{\alpha\beta}^0$ is the residual strain component due to thermal contraction and is assumed to have the form

$$\varepsilon_{\alpha\beta}^0(x) = \left[1 - \exp\left(-\frac{x}{l_0}\right)\right]\varepsilon_T \delta_{\alpha\beta} \tag{5}$$

where ε_T represents the amplitude of the isotropic thermal compression, and l_0 is a characteristic length for the compression release due to the free edge of the film caused by the crack. We did not directly solve eqs 1 and 2. Instead, we used an iterative scheme of solving the kinetic equations via gradient flow[23,48,49] to find that the stationary variation of the total elastic energy with respect to the middle-plane displacement leads to in-plane and out-of-plane equilibrium equations in the film. The steady solutions of the kinetic equations based on gradient flow give the equilibrium configuration of the coupled nonlinear eqs 1 and 2. The convergence insensitive to the geometry of the thickness-gradient FvK plate is driven by monotonically decreasing the total elastic energy. The details of the calculation are outlined in the part of nonlinear wrinkling simulation in the Supporting Information. Note that the finite deformation of the compliant substrate leads to the wrinkling wavelength and amplitude depending on the strain.[50,51] In the current treatment the compliant substrate is considered in a small deformation limit, which is valid when the compressive strain is not very big. Large compressive strain may also cause delamination and result in the transition from wrinkling to buckle-delamination.[49] In our experiment we can control the amplitude of the compression by appropriate cooling. Furthermore, the interfacial adhesion between the metal film and the PDMS was improved greatly due to the bombardment from high-energy particles and the radiation from plasma during deposition. The wrinkling-induced delamination is thus suppressed and not observed in our experiment. Therefore, in the above modeling we assume there is no delamination as indicated by the displacement being continuous across the interface between the film and the substrate.

Figure 3 shows the typical simulated wrinkling patterns of the thickness-gradient film wherein $l_0 = 200h^*$, $h^* = 50$ nm, $h(x) = h^*(1 - \alpha(x/h^*))$ with $\alpha = 1/4096$, $\mu_f/\mu_s = 2 \times 10^3$, $\nu_f = 0.3$, and $\nu_s = 0.5$. The critical wrinkling strain is $\varepsilon_w = [4(1 + \nu_f)]^{-1}[(3\ \mu_s(1 - \nu_f))/(\mu_f(1 - \nu_s))]^{2/3} = 0.32\%$. The equally biaxial compression $\varepsilon_T = 1.3\%$ is set to be 4 times that of the

critical wrinkling strain. Figure 3a demonstrates the global profile of the wrinkling patterns with the computational domain size of $4096h^* \times 512h^*$. Figure 3b−e shows the sections of the wrinkling patterns with the size of $1024h^* \times 1024h^*$ starting from $x = 0h^*$, $1024h^*$, $2048h^*$, and $3072h^*$, respectively. Clearly, the simulated wrinkling patterns show the feature of coexisting branched straight stripes, herringbones, and labyrinths along the gradient direction, in excellent agreement with the observed wrinkles shown in Figure 2.

Figure 4 further plots the average short wavelength and the average root square deflection amplitude $R_a/h^* = \langle(\zeta^2)^{1/2}\rangle/h^*$ as a function of x, where the upper row represents the experimental results obtained from Figure 2, while the lower row represents the simulated results obtained from Figure 3. Both Figure 4a,c show that the wavelength decreases approximately linearly with the distance, and the decay curve is not smooth but step-shaped. The step-shaped feature of the wavelength is mainly due to the branching behavior of the stripe wrinkles. In Figures 2 and 3, at least three collective bifurcation behaviors of the stripe wrinkles can be seen clearly, corresponding to the three steps of the curves shown in Figure 4a,c. The analysis of strain energy minimization including the film stretching and bending energies and the substrate elastic energy shows that one-dimensional equilibrium wrinkle wavelength and amplitude obey the following scaling laws, for example, $\lambda(x) \propto 2\pi h(x)[(\mu_f(1 - \nu_s))/(3\mu_s(1 - \nu_f))]^{1/3}$ and $A(x) \propto h(x)(\sigma^0/\sigma_w - 1)^{1/2}$ with $\sigma^0 = \bar{E}_f(x)\varepsilon_{xx}^0(x)$ and σ_w the critical wrinkling membrane stress. σ_w decreases nonlinearly with the decrease of the film thickness.[45] The scaling law of $\lambda(x)$ on $h(x)$ showing the linear change of the wavelength with the film thickness is consistent with that of the plots in Figure 4a,c. This has also been reported in other gradient film−substrate systems under uniaxial loading.[43−46] However, the plot of $A(x)$ versus $h(x)$ in Figure 4b,d shows a plateau followed by the monotonic decrease, different from that in the system under uniaxial compression.[45] The existence of the plateau is consistent with the fact that the amplitude changes slightly with respect to the change of the distance x shown in Supporting Information, Figure S1c. In our analysis we assume the thickness of the substrate is much thicker than the metal film. The obtained scaling laws of the wrinkling wavelength and amplitude are consistent with the experimental observations. In fact the compressibility and the thickness of the compliant substrate significantly affect the forms of these scaling laws.[52] We may regulate the wrinkling pattern through them.

Although the wrinkling patterns of the gradient-film under biaxial compression is more complex than those under uniaxial compression, the simulated results in Figure 5 show that the wrinkling patterns of the film under biaxial compression can be roughly viewed as a superposition of the film under uniaxial loadings perpendicular and parallel to the gradient direction. Figure 5b shows that when the gradient-film under the uniaxial compression is perpendicular to the gradient direction, hierarchical straight stripe wrinkles parallel to the gradient direction form in the whole region, and the local wrinkling wavelength and amplitude decrease with decreasing the local film thickness. The change of the wavelength with respect to the thickness is discontinuous since it depends on the condition of the wrinkling-branching instability. Our previous study confirmed that the wrinkling-branching instability occurs only when the characteristic length of the membrane stiffness inhomogeneity zone was larger than the coherency persistent length.[48] Figure 5c shows that when the film under uniaxial
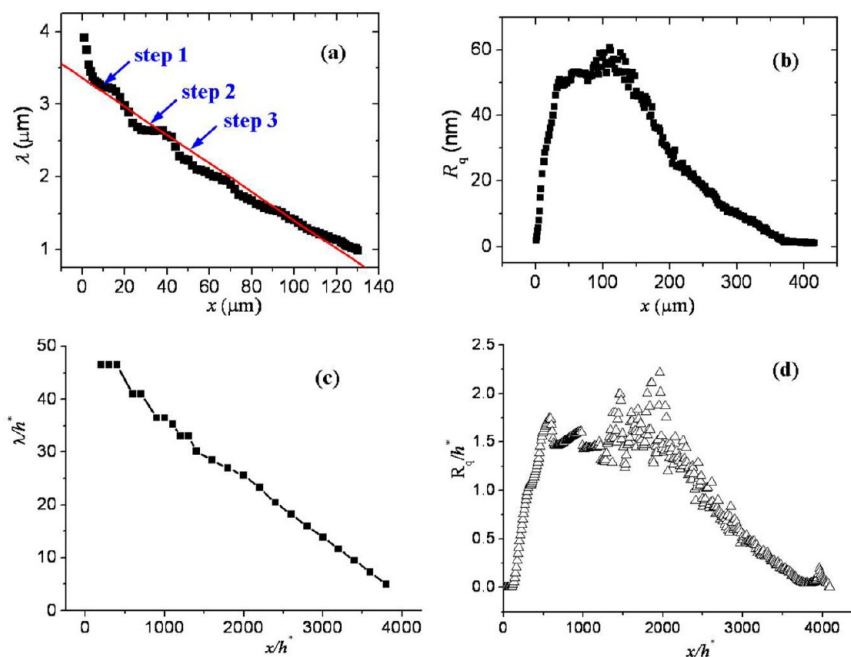

Figure 3. Simulated sequential profiles of the wrinkling patterns in the film with thickness gradient of 1/4096. (a) The profile with the computational domain size of $4096h^* \times 512h^*$. (b−e) The profiles with the size of $1024h^* \times 1024h^*$ starting from $x = 0h^*$, $1024h^*$, $2048h^*$, and $3072h^*$, respectively. The circle in Figure 4c denotes the vertically aligned stripe wrinkles.

Figure 4. Plots of the average short wavelength (a,c) and the average root square deflection amplitude (b,d) of the wrinkling patterns as a function of distance x. (a,b) The experimental results obtained from Figure 2. (c,d) The simulated results obtained from Figure 3
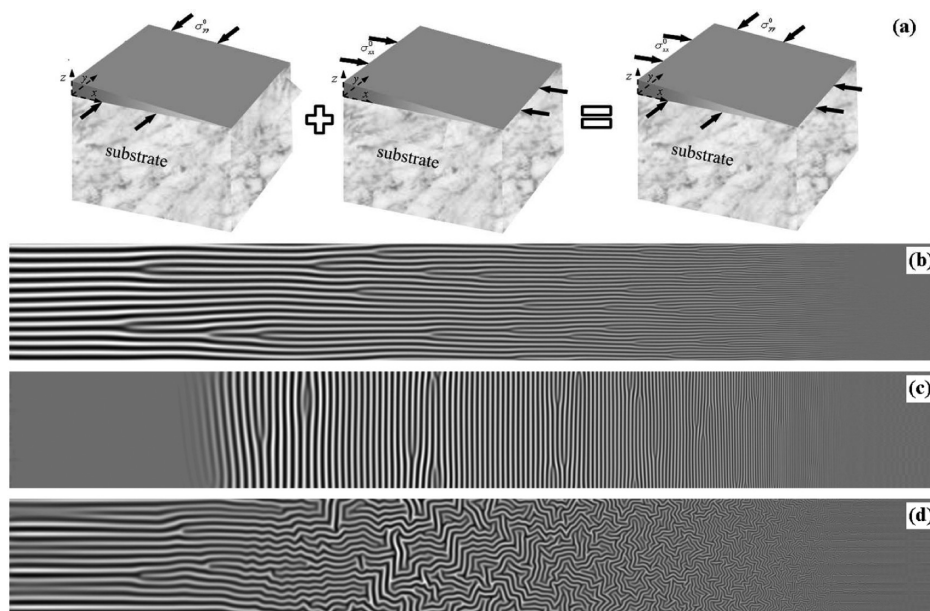
Figure 5. (a) The sketch for biaxially compressed thickness-gradient film understood as the combination of the thickness-gradient film under uniaxial loadings perpendicular and parallel to the gradient direction. (b−d) Simulated wrinkling morphologies of the film under the uniaxial loading perpendicular to the gradient direction, the uniaxial loading parallel to the gradient direction, and the biaxial loading, respectively.

compression is parallel to the gradient direction, the simulated wrinkling patterns exhibit straight stripe wrinkles perpendicular to the gradient direction. Interestingly, these stripe wrinkles first occur at the location with minimum film thickness and then progressively grow into the thicker film region. Usually, the wrinkles cannot extend into the entire region of the film, while they can for the film under uniaxial compression perpendicular to the gradient direction. Figure 5d shows the simulated wrinkling patterns in the gradient film under equi-biaxial compression. In comparison with Figure 5b−d, we found that the formation of branched stripe wrinkles is due to the contribution of the compression perpendicular to the

gradient direction. The transition of the straight stripes into herringbone patterns is attributed to the fact that the compression parallel to the gradient direction tries to direct the wrinkles perpendicular to the gradient direction and thus destabilize the wrinkles parallel to the gradient direction. When the distance x increases, the competition between the compressions along and perpendicular to the gradient direction is comparable, and there is a frustration of the wrinkle orientation, and thus labyrinthlike wrinkling patterns form. Although we now know that the wrinkling patterns in Figure 5d can be viewed as a superposition of the patterns in Figure 5b,c,
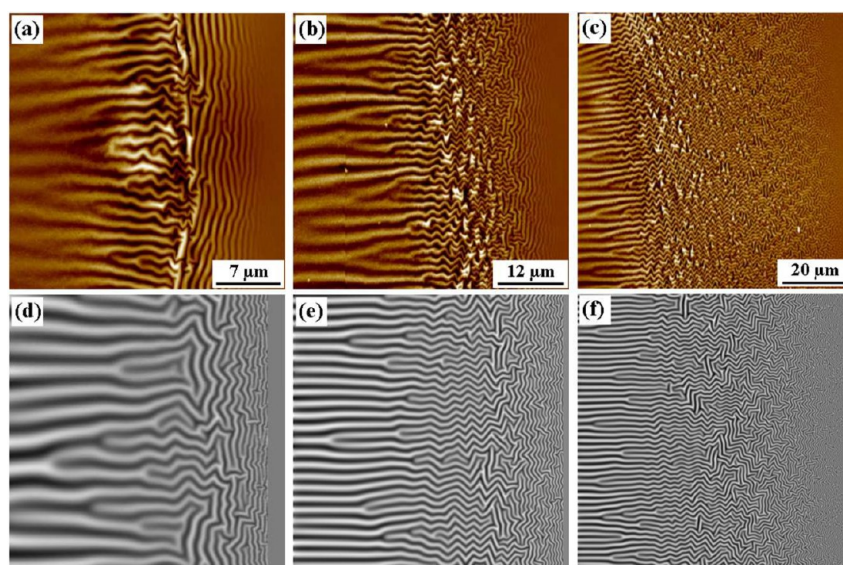
Figure 6. Comparison between simulations and experiments for the wrinkling morphologies of the biaxially compressed film with varied thickness gradients. (a−c) The experimental observations with decreasing the thickness gradient. The slopes (defined as h_{max}/w) are ∼2.5×10^{-3}, 1.4×10^{-3}, and 0.6×10^{-3}, respectively. (d−f) The simulated results with thickness gradients of 1/512, 1/1024, and 1/2048 in the computational domains of $512l \times 512l$, $1024l \times 1024l$, and $2048l \times 2048l$, respectively.

it is not additive due to the nonlinearity of the thin plate deformation.

By performing the simulations of the wrinkles in the corresponding gradient film under uniaxial compression we found that the change of the thickness gradient not only affects the orientation, the wavelength, and amplitude of the wrinkles but also changes the region where the wrinkles occur. For example, we found that under large thickness gradient the compression parallel to the gradient direction leads to the wrinkles perpendicular to the gradient direction accumulated in the area with thinner film thickness, while the compression perpendicular to the gradient direction leads to the wrinkles parallel to the gradient direction accumulated in the area with thicker film thickness. As the thickness gradient decreases, the transition boundary becomes wider. In the boundary the competition between the uniaxial loadings perpendicular and parallel to the gradient direction to orient stripe wrinkle is comparable, and the orientation of the stripe wrinkle is frustrated; this is why herringbone and labyrinth wrinkling patterns arise. In the limit of zero thickness gradient, the boundary extends to the whole film, and the wrinkles in such film exhibit no directional preference. On the basis of the above discussion, we anticipated that various wrinkling patterns can form by tuning the interplay between the biaxial compression and the thickness gradient.

To investigate the effect of thickness gradient on the wrinkling patterns, a special wedge-shaped film with varied slopes was prepared by continuously changing the distance from the shutter to the PDMS substrate during deposition. In detail, one end of the shutter touched to the PDMS surface (i.e., the distance $d = 0$), while the other was above several millimeters from the PDMS surface, as shown in Supporting Information, Figure S3. The width of the wrinkled film region w increases obviously with increasing the distance d (Figure S3). Because the maximum film thickness is uniform, the thickness gradient (i.e., the wedge slope, which is roughly defined as h_{max}/w) decreases greatly with increasing the distance d. The typical wrinkle morphologies of the film (here is iron) with varied

thickness gradients are shown in Figure 6a−c and Supporting Information, Figure S4. In the presence of large thickness gradient (Figure 6a), the wrinkle under equi-biaxial compression exhibits a stripelike pattern with a clear transition boundary from parallel to perpendicular to the thickness gradient direction as the thickness decreases. The profiles of the stripes parallel and perpendicular to the gradient direction show that they are both periodic (Supporting Information, Figure S5a). The amplitude of the stripes parallel to the gradient direction is almost unchanged because the film thickness along this profile line is uniform, while the amplitude of the stripes perpendicular to the gradient direction decays because the film thickness decreases gradually. When the thickness gradient decreases (Figures 6b,c), the stripes perpendicular to the thickness gradient direction degenerate gradually, and finally completely disordered labyrinth pattern forms (Supporting Information, Figure S6). Meanwhile, the transition boundary is significantly broadened with the appearance of herringbone and labyrinth zones. Figure 6d−f shows the simulated results of the wrinkles with decreasing the thickness gradient. The striking agreement between the simulations and the experimental observations shown in Figure 6 not only confirms the formation mechanism of such hierarchical wrinkling patterns but also demonstrates that they can be designed via controlled thickness gradient. The ability to tune the highly ordered wrinkling patterns through controlling thickness gradient makes these wrinkles excellent candidates for tunable multifunctional surface properties such as anisotropic liquid flow, friction, adhesion, wetting or dewetting, reflectivity, stamp, cell growth, etc.

The results obtained here also reveal that tunable nonlinear wrinkles in metal films on soft elastic substrates are attributed to the interplay between biaxial compression and thickness gradient. The equilibrium wrinkle such as the wavelength, the amplitude, and the pattern is determined by minimizing the total elastic energies in the film and the substrate. The total elastic energy usually has a complex relationship with film thickness, residual compression, and the modulus ratio between

the film and the substrate. In the homogeneous compressed film with constant thickness numerical analysis shows that the nonlinear wrinkles can evolve into stripes, zigzag, or labyrinths, depending on the anisotropy of the compression.[30] The presence of thickness gradient in the film may change the homogeneous isotropic compression into anisotropic and positionally dependent compression. The resultant wrinkle patterns are spatially dependent with coexisting branched stripes, zigzag, and labyrinths. The nonlinear wrinkling analysis based on numerical simulation explicitly takes into account the effect of thickness gradient and may offer a computational tool to elucidate the wrinkling pattern in gradient films.

VI. CONCLUSIONS

In summary, metal films with controlled thickness gradient deposited on PDMS substrates have been prepared via direct current magnetron sputtering and placing a shutter between the substrate and the target during deposition. Various spontaneous formations of hierarchical ordered wrinkling patterns are observed and discussed in detail. The coexisting branched stripes, herringbones, and labyrinths along the direction of thickness decrease are the result of the competition between the compressions along and perpendicular to the thickness gradient direction, which is validated by our numerical simulation based on nonlinear wrinkling model. We anticipate that the thickness-gradient films deposited on soft elastic substrates will provide a platform for the fundamental researches on various wrinkle morphologies including branched stripes, herringbones, and labyrinths and their coexistence and transitions with each other. The experiment technique presented in this paper can also be developed to effectively maneuver the pattern formation and transition, which may be beneficial for the technological applications in optical devices, microelectro-mechanical systems, fluid handling systems, biological templates, etc.

■ ASSOCIATED CONTENT

Ⓢ Supporting Information

Nonlinear wrinkling simulation; evolution behaviors of the wrinkling patterns with decreasing the film thickness in a thickness-gradient film; preparation of a wedged film with varied thickness gradients; details of the wrinkle morphologies and profiles under different thickness gradients. This material is available free of charge via the Internet at http://pubs.acs.org.

■ AUTHOR INFORMATION

Corresponding Authors
*E-mail: sjyu@cjlu.edu.cn. (S.-J. Yu).
*E-mail: yni@ustc.edu.cn. (Y. Ni).

Notes
The authors declare no competing financial interest.

■ ACKNOWLEDGMENTS

■ REFERENCES

(1) Efimenko, K.; Rackaitis, M.; Manias, E.; Vaziri, A.; Mahadevan, L.; Genzer, J. Nested Self-Similar Wrinkling Patterns in Skins. *Nat. Mater.* **2005**, *4*, 293−297.

(2) Genzer, J.; Groenewold, J. Soft Matter with Hard Skin: From Skin Wrinkles to Templating and Material Characterization. *Soft Matter* **2006**, *2*, 310−323.

(3) Li, B.; Cao, Y. P.; Feng, X. Q.; Gao, H. J. Mechanics of Morphological Instabilities and Surface Wrinkling in Soft Materials. *Soft Matter* **2012**, *8*, 5728−5745.

(4) Allen, H. G. *Analysis and Design of Structural Sandwich Panels*; Pergamon Press: Oxford, U.K., 1969.

(5) Groenewold, J. Wrinkling of Plates Coupled with Soft Elastic Media. *Phys. A* **2001**, *298*, 32−45.

(6) Yang, S.; Khare, K.; Lin, P. C. Harnessing Surface Wrinkle Patterns in Soft Matter. *Adv. Funct. Mater.* **2010**, *20*, 2550−2564.

(7) Khang, D. Y.; Rogers, J. A.; Lee, H. H. Mechanical Buckling: Mechanics, Metrology, and Stretchable Electronics. *Adv. Funct. Mater.* **2009**, *19*, 1526−1536.

(8) Ohzono, T.; Monobe, H.; Shiokawa, K.; Fujiwara, M.; Shimizu, Y. Shaping Liquid on A Micrometre Scale Using Microwrinkles as Deformable Open Channel Capillaries. *Soft Matter* **2009**, *5*, 4658−4664.

(9) Chan, E. P.; Smith, E. J.; Hayward, R. C.; Crosby, A. J. Surface Wrinkles for Smart Adhesion. *Adv. Mater.* **2009**, *20*, 711−716.

(10) Vajpayee, S.; Khare, K.; Yang, S.; Hui, C. Y.; Jagota, A. Adhesion Selectivity Using Rippled Surfaces. *Adv. Funct. Mater.* **2011**, *21*, 547−555.

(11) Chung, J. Y.; Youngblood, J. P.; Stafford, C. M. Anisotropic Wetting on Tunable Micro-Wrinkled Surfaces. *Soft Matter* **2007**, *3*, 1163−1169.

(12) Chan, E. P.; Kundu, S.; Lin, Q.; Stafford, C. M. Quantifying The Stress Relaxation Modulus of Polymer Thin Films via Thermal Wrinkling. *ACS Appl. Mater. Interfaces* **2011**, *3*, 331−338.

(13) Yu, C.; O'Brien, K.; Zhang, Y. H.; Yu, H.; Jiang, H. Tunable Optical Gratings Based on Buckled Nanoscale Thin Films on Transparent Elastomeric Substrates. *Appl. Phys. Lett.* **2010**, *96*, 041111.

(14) Efimenko, K.; Finlay, J.; Callow, M. E.; Genzer, J. Development and Testing of Hierarchically Wrinkled Coatings for Marine Antifouling. *ACS Appl. Mater. Interfaces* **2009**, *1*, 1031−1040.

(15) Kim, J. B.; Kim, P.; Pégard, N. C.; Oh, S. J.; Kagan, C. R. Wrinkles and Deep Folds as Photonic Structures in Photovoltaics. *Nat. Photonics* **2012**, *6*, 327−332.

(16) Vandeparre, H.; Gabriele, S.; Brau, F.; Gay, C.; Parker, K. K.; Damman, P. Hierarchical Wrinkling Patterns. *Soft Matter* **2010**, *6*, 5751−5756.

(17) Yoo, P. J.; Suh, K. Y.; Park, S. Y.; Lee, H. H. Physical Self-Assembly of Microstructures by Anisotropic Buckling. *Adv. Mater.* **2002**, *14*, 1383−1387.

(18) Bowden, N.; Brittain, S.; Evans, A. G.; Hutchinson, J. W.; Whitesides, G. M. Spontaneous Formation of Ordered Structures in Thin Films of Metals Supported on An Elastomeric Polymer. *Nature* **1998**, *393*, 146−149.

(19) Bowden, N.; Huck, W. T. S.; Paul, K. E.; Whitesides, G. M. The Controlled Formation of Ordered, Sinusoidal Structures by Plasma Oxidation of An Elastomeric Polymer. *Appl. Phys. Lett.* **1999**, *75*, 2557−2559.

(20) Huntington, M. D.; Engel, C. J.; Hryn, A. J.; Odom, T. W. Polymer Nanowrinkles with Continuously Tunable Wavelengths. *ACS Appl. Mater. Interfaces* **2013**, *5*, 6438−6442.

(21) Vandeparre, H.; Damman, P. Wrinkling of Stimuloresponsive Surfaces: Mechanical Instability Coupled to Diffusion. *Phys. Rev. Lett.* **2008**, *101*, 124301.

(22) Velankar, S. S.; Lai, V. Swelling-Induced Delamination Causes Folding of Surface-Tethered Polymer Gels. *ACS Appl. Mater. Interfaces* **2012**, *4*, 24−29.

(23) Ni, Y.; He, L. H.; Liu, Q. H. Modeling Kinetics of Diffusion-Controlled Surface Wrinkles. *Phys. Rev. E* **2011**, *84*, 051604.

(24) Chung, J. Y.; Nolte, A. J.; Stafford, C. M. Diffusion-Controlled, Self-Organized Growth of Symmetric Wrinkling Patterns. *Adv. Mater.* 2009, *21*, 1358−1362.

(25) Lucantonio, A.; Roché, M.; Nardinocchi, P.; Stone, H. A. Buckling Dynamics of A Solvent-Stimulated Stretched Elastomeric Sheet. *Soft Matter* 2014, *10*, 2800−2804.

(26) Takahashi, M.; Maeda, T.; Uemura, K.; Yao, J.; Tokuda, Y.; Yoko, T.; Kaji, H.; Marcelli, A.; Innocenzi, P. Photoinduced Formation of Wrinkled Microstructures with Long-Range Order in Thin Oxide Films. *Adv. Mater.* 2007, *19*, 4343−4346.

(27) Yang, D.; He, L. H. Photo-Triggered Wrinkling of Glassy Nematic Films. *Smart Mater. Struct.* 2014, *23*, 045012.

(28) Huang, J.; Juszkiewicz, M.; de Jeu, W. H.; Cerda, E.; Emrick, T.; Menon, N.; Russell, T. P. Capillary Wrinkling of Floating Thin Polymer Films. *Science* 2007, *317*, 650−653.

(29) Zhang, P.; Yang, D.; Li, Z.; Ma, H. Controlled Wrinkle Formation via Bubble Inflation Strain Engineering. *Soft Matter* 2010, *6*, 4580−4584.

(30) Huang, Z. Y.; Hong, W.; Suo, Z. Nonlinear Analyses of Wrinkles in A Film Bonded to A Compliant Substrate. *J. Mech. Phys. Solids* 2005, *53*, 2101−2118.

(31) Chen, X.; Hutchinson, J. W. Herringbone Buckling Patterns of Compressed Thin Films on Compliant Substrates. *J. Appl. Mech.* 2004, *71*, 597−603.

(32) Cai, S.; Breid, D.; Crosby, A. J.; Suo, Z.; Hutchinson, J. W. Periodic Patterns and Energy States of Buckled Films on Compliant Substrates. *J. Mech. Phys. Solids* 2011, *59*, 1094−1114.

(33) Audoly, B.; Boudaoud, A. Buckling of A Stiff Film Bound to A Compliant Substrate—Part I: Formulation, Linear Stability of Cylindrical Patterns, Secondary Bifurcations. *J. Mech. Phys. Solids* 2008, *56*, 2401−2421.

(34) Mahadevan, L.; Rica, S. Self-Organized Origami. *Science* 2005, *307*, 1740.

(35) Lin, P. C.; Yang, S. Spontaneous Formation of One-Dimensional Ripples in Transit to Highly Ordered Two-Dimensional Herringbone Structures through Sequential and Unequal Biaxial Mechanical Stretching. *Appl. Phys. Lett.* 2007, *90*, 241903.

(36) Yin, J.; Yagüe, J. L.; Eggenspieler, D.; Gleason, K. K.; Boyce, M. C. Deterministic Order in Surface Micro-Topologies through Sequential Wrinkling. *Adv. Mater.* 2012, *24*, 5441−5446.

(37) Yin, J.; Yagüe, J. L.; Boyce, M. C.; Gleason, K. K. Biaxially Mechanical Tuning of 2-D Reversible and Irreversible Surface Topologies through Simultaneous and Sequential wrinkling. *ACS Appl. Mater. Interfaces* 2014, *6*, 2850−2857.

(38) Huck, W. T. S.; Bowden, N.; Onck, P.; Pardoen, T.; Hutchinson, J. W.; Whitesides, G. M. Ordering of Spontaneously Formed Buckles on Planar Surfaces. *Langmuir* 2000, *16*, 3497−3501.

(39) Vandeparre, H.; Léopoldès, J.; Poulard, C.; Desprez, S.; Derue, G.; Gay, C.; Damman, P. Slippery or Sticky Boundary Conditions: Control of Wrinkling in Metal-Capped Thin Polymer Films by Selective Adhesion to Substrates. *Phys. Rev. Lett.* 2007, *99*, 188302.

(40) Ding, W.; Yang, Y.; Zhao, Y.; Jiang, S.; Cao, Y.; Lu, C. Well-Defined Orthogonal Surface Wrinkles Directed by the Wrinkled Boundary. *Soft Matter* 2013, *9*, 3720−3726.

(41) Vandeparre, H.; Piñeirua, M.; Brau, F.; Roman, B.; Bico, J.; Gay, C.; Bao, W.; Lau, C. N.; Reis, P. M.; Damman, P. Wrinkling Hierarchy in Constrained Thin Sheets from Suspended Graphene to Curtains. *Phys. Rev. Lett.* 2011, *106*, 224301.

(42) Yu, S. J.; Zhang, Y. J.; Zhou, H.; Chen, M. G.; Zhang, X. F.; Jiao, Z. W.; Si, P. Z. Spontaneous Formation of Hierarchical Wrinkles in Cr Films Deposited on Silicone Oil Drops with Constrained Edges. *Phys. Rev. E* 2013, *88*, 042401.

(43) Stafford, C. M.; Harrison, C.; Beers, K. L.; Karim, A.; Amis, E. J.; Vanlandingham, M. R.; Kim, H. C.; Volksen, W.; Miller, R. D.; Simonyi, E. E. A Buckling-Based Metrology for Measuring the Elastic Moduli of Polymeric Thin Films. *Nat. Mater.* 2004, *3*, 545−550.

(44) Claussen, K. U.; Tebbe, M.; Giesa, R.; Schweikart, A.; Fery, A.; Schmidt, H. W. Towards Tailored Topography: Facile Preparation of Surface-Wrinkled Gradient Poly (Dimethyl Siloxane) with Continuously Changing Wavelength. *RSC Adv.* 2012, *2*, 10185−10188.

(45) Yin, J.; Chen, X. Elastic Buckling of Gradient Thin Films on Compliant Substrates. *Philos. Mag. Lett.* 2010, *90*, 423−433.

(46) Noroozi, M.; Jiang, L. Buckling and Wrinkling of A Functionally Graded Material (FGM) Thin Film. *Int. J. Appl. Mech.* 2012, *4*, 1250012.

(47) Mansfield, E. H. *The Bending and Stretching of Plates,* 2nd ed.; Cambridge Univ. Press: Cambridge, U.K., 1989.

(48) Ni, Y.; Yang, D.; He, L. H. Spontaneous Wrinkle Branching by Gradient Stiffness. *Phys. Rev. E* 2012, *86*, 031604.

(49) Pan, K.; Ni, Y.; He, L. H.; Huang, R. Nonlinear Analysis of Compressed Elastic Thin Films on Elastic Substrates: From Wrinkling to Buckle-Delamination. *Int. J. Solids Struct.* 2014, *51*, 3715−3726.

(50) Jiang, H.; Khang, D. Y.; Song, J.; Sun, Y.; Huang, Y.; Rogers, J. A. Finite Deformation Mechanics in Buckled Thin Films on Compliant Supports. *Proc. Natl. Acad. Sci. U. S. A.* 2007, *104*, 15607−15612.

(51) Song, J.; Jiang, H.; Liu, Z. J.; Khang, D. Y.; Huang, Y.; Rogers, J. A.; Lu, C.; Koh, C. G. Buckling of A Stiff Thin Film on A Compliant Substrate in Large Deformation. *Int. J. Solids Struct.* 2008, *45*, 3107−3121.

(52) Li, B.; Huang, S. Q.; Feng, X. Q. Buckling and Postbuckling of A Compressed Thin Film Bonded on A Soft Elastic Layer: A Three-Dimensional Analysis. *Arch. Appl. Mech.* 2010, *80*, 175−188.